Journal of the Indian Chemical Society 98 (2021) 100116

Contents lists available at ScienceDirect

Journal of the Indian Chemical Society

journal homepage: www.editorialmanager.com/JINCS/default.aspx

A new strategy to improve catalytic activity for chlorinated volatile organic compounds oxidation over cobalt oxide: Introduction of strontium carbonate

Hao Liu [a], Kai Shen [a], Hailin Zhao [a], Yongjun Jiang [a], Yanglong Guo [a,**], Yun Guo [a], Li Wang [a], Wangcheng Zhan [a,b,*]

[a] Key Laboratory for Advanced Materials and Research Institute of Industrial Catalysis, School of Chemistry & Molecular Engineering, East China University of Science and Technology, Shanghai, 200237, PR China

[b] Frontiers Science Center for Materiobiology and Dynamic Chemistry, East China University of Science and Technology, Shanghai, 200237, PR China

ARTICLE INFO

Keywords:
Catalytic combustion
Vinyl chloride
Cobalt oxides
Alkaline-earth metal salts

ABSTRACT

Co_3O_4–$SrCO_3$ catalysts with various Sr/Co ratios were synthesized by the coprecipitation method, and their properties were tuned by adjusting the Sr/Co molar ratio. Furthermore, the catalytic combustion of vinyl chloride (VC) was used to evaluate the catalytic activity of the Co_3O_4–$SrCO_3$ catalysts. The physicochemical properties of the catalysts were studied by X-ray diffraction (XRD), infrared spectroscopy (IR), N_2 sorption, scanning electron microscopy (SEM), X-ray photoelectron spectroscopy (XPS), transmission electron microscopy (TEM), H_2 temperature-programmed reduction (H_2-TPR) and VC temperature-programmed desorption (VC-TPD). The results showed that the Co_3O_4–$SrCO_3$ catalysts exhibited composite phases of Co_3O_4 and $SrCO_3$ and the presence of interactions between them. As a result, the crystallization of the Co_3O_4 phase for the Co_3O_4–$SrCO_3$ catalysts was restrained, and the state of Co on the catalyst surface was adjusted. Furthermore, the reducibility and VC adsorption capacity of the Co_3O_4–$SrCO_3$ catalysts with Sr/Co molar ratios of 0.2 and 0.4 were enhanced compared with those of the Co_3O_4 catalyst. Otherwise, catalyst SrCo-0.4 exhibited excellent catalytic performance, accompanied by the highest reaction rate and the lowest apparent activation energy. More importantly, the optimized $SrCO_3$–Co_3O_4 catalyst showed superior catalytic performance compared with other transition metal oxides in previous literature. These results brought a new idea for promoting the activity of transition metal catalysts for the deep oxidation of chlorinated volatile organic compounds (CVOCs) by introducing alkaline-earth metal salts.

1. Introduction

Following the expeditious expansion of the chemical industry, the emission of volatile organic compounds (VOCs) has caused severe threats to the security of human health and the atmosphere. Thus, it is urgent to develop efficient methods to eliminate the emission of VOCs. As one class of VOCs, chlorinated volatile organic compounds (CVOCs) have attracted sufficient attention from researchers due to their high toxicity and high emission. Catalytic combustion is an efficient technology to eliminate CVOCs emissions because of the advantages of desirable high efficiency and no secondary pollution [1–6]. Until now, noble metal-based catalysts, transition metal oxides and molecular sieve catalysts have been applied for the oxidation of CVOCs emissions. Among these catalysts, transition metal oxides have received increasing attention owing to their inexpensive materials, simple preparation and high stability [7–15]. For example, the $LaMnO_3$ catalyst shows excellent catalytic performance for the oxidation of vinyl chloride (VC) due to its stable structure, strong reducibility of Mn^{4+} and redox cycling between Mn^{4+} and Mn^{3+} [16,17]. In addition, CeO_2-based catalysts also exhibit significantly high activity for CVOCs oxidation due to excellent redox properties and abundant oxygen vacancies on their surface [18,19].

Compared to other transition metal oxides, Co_3O_4-based catalysts

* Corresponding author. Key Laboratory for Advanced Materials and Research Institute of Industrial Catalysis, School of Chemistry & Molecular Engineering, East China University of Science and Technology, Shanghai, 200237, PR China.
** Corresponding author.
E-mail addresses: ylguo@ecust.edu.cn (Y. Guo), zhanwc@ecust.edu.cn (W. Zhan).

https://doi.org/10.1016/j.jics.2021.100116
Received 31 March 2021; Received in revised form 21 July 2021; Accepted 22 July 2021

show superior catalytic activity and stability for VC oxidation. VC first adsorbs on Co^{2+} sites by forming a π-complex between C═C and the surface Co^{2+} ions (acting as Lewis acid sites) [20,21]. Subsequently, the active oxygen species on the surface attack the adsorption intermediate and oxidize hydrocarbon species to carbon dioxide and water. Moreover, the Cl species occupy the oxygen vacancy on the surface and desorb at high temperature. Finally, the formed oxygen vacancy is replenished by oxygen in the air. Based on this reaction mechanism, optimizing the preparation method and doping other transition metals are common strategies to improve the catalytic performance of Co_3O_4 catalysts. Yuan et al. [22] prepared Co_3O_4 oxide catalysts by different synthetic routes and found that the Co_3O_4-TP catalyst (template method) showed a high catalytic activity due to its enhanced oxygen mobility and abundant adsorbed oxygen species generated from surface defects of the Co_3O_4-TP catalyst. Wang et al. [23] adopted a metal-doping method to prepare a RuO_x/Co_3O_4 catalyst and found that the great activity could be attributed to the excellent reducibility due to abundant oxygen vacancies originating from Ru^{4+} species entering the Co_3O_4 lattice. Although researchers have made substantial achievements in improving the catalytic performance of Co_3O_4-based catalysts for VC deep oxidation, the development of novel strategies capable of enhancing the catalytic performance of Co_3O_4-based catalysts is still highly desirable.

Herein, this is the first study to introduce strontium carbonate into a Co_3O_4 oxide catalyst, aiming to improve its catalytic performance for the deep oxidation of vinyl chloride. The corresponding $SrCO_3$–Co_3O_4 composite catalysts were synthesized by the coprecipitation method, and the ratio of Sr/Co was tuned. The physicochemical properties of the catalysts were studied by various characterizations and their catalytic performances for the deep oxidation of VC were evaluated. Compared with the Co_3O_4 catalyst, the $SrCO_3$–Co_3O_4 catalysts showed better catalytic performances and selectivity for the deep oxidation of VC. Our findings provide a novel strategy for enhancing the catalytic performance of Co_3O_4-based catalysts in VC oxidation by combining with metal salts instead of metal oxides.

2. Experimental

2.1. Preparation of $SrCO_3$–Co_3O_4 catalysts

$SrCO_3$–Co_3O_4 composite catalysts were prepared through a coprecipitation method. Typically, stoichiometric $Sr(NO)_2$ and $Co(NO)_2{\cdot}H_2O$ were first added to 100 mL of deionized water, and then 50 mL of ammonium oxalate solution was added dropwise until the colour of the mixed solution became clear. After the resulting solution was aged for 8 h at room temperature, the precipitate was collected by filtration, washed with deionized water, dried at 60 °C for 12 h, and then calcined at 500 °C for 3 h in air. The obtained catalysts were marked as SrCo-x, in which x presented molar ratios of Sr and Co of 0.2, 0.4 and 1, respectively. The $SrCO_3$ and Co_3O_4 samples were also synthesized by the same method as the reference catalysts.

2.2. Characterization of catalysts

All the $SrCO_3$–Co_3O_4 composite catalysts were analysed using X-ray diffraction (XRD) technology on a Bruker AXS D8 Focus diffractometer with Cu Kα radiation (40 kV and 40 mA) to confirm their crystal structure. Standard database cards (JCPDS) were used to identify the phases of the catalysts. N_2 adsorption and desorption measurements were processed to detect the specific surface area. The experiment was conducted at 77 K on a Micromeritics ASAP 2020 M apparatus. The specific surface area (SSA) of the catalyst was calculated by the Brunauer-Emmett-Teller (BET) method. The SEM images were obtained using a Nova Nano SEM 450 microscope operated at 15 kV. The morphology of the catalysts was detected by scanning transmission electron microscopy (STEM) with a ThermoFisher Talos F200X and high angle annular dark-field (HAADF)-STEM with a convergence semi-angle of 11 mrad and inner and outer collection angles of 59 and 200 mrad, respectively. The distribution of elements on the surface was recorded by energy-dispersive X-ray spectroscopy (EDS) with 4 in-column Super-X detectors. The FT-IR spectra of the $SrCO_3$–Co_3O_4 composite catalyst were recorded on a Nicolet Nexus 670 spectrometer. Before scanning, the sample was mixed with KBr powder. The states of the surface elements were analysed by X-ray photoelectron spectroscopy (XPS). The instrument used was a Thermo-Fisher ESCALAB 250Xi electron spectrometer equipped with Al Kα (1486.6 eV) radiation. Before the experiments, all the samples were baked in a drying oven at 100 °C.

The reducibility of catalysts was tested by temperature-programmed reduction of H_2 (H_2-TPR) technology. The experiment was operated on a PX200 apparatus with a thermal conductivity detector (TCD). Each sample (50 mg) was pretreated in N_2 flow for 60 min at 200 °C. Then, after cooling to 25 °C, the gas was switched to 40 mL/min H_2/Ar mixed gas, and the sample was heated from 25 °C to 500 °C with a step of 10 °C/min.

The VC adsorption capacity of the catalysts was detected by temperature-programmed desorption of vinyl chloride (VC-TPD) experiments. The instrument used was a Ruimin 2060 gas chromatograph with a thermal conductivity detector (TCD). The catalyst (20 mg) was pretreated in a N_2 flow of 40 mL/min for 60 min at 200 °C. Then, after cooling to 25 °C, vinyl chloride/N_2 mixed gas (1000 ppm VC) was introduced for 30 min. After saturation adsorption, N_2 gas (60 mL/min) was introduced and kept for 60 min to remove physically adsorbed vinyl chloride on the catalyst surface. Finally, the catalyst was heated from 25 °C to 500 °C at a heating rate of 10 °C/min, and outlet gas was detected by TCD.

2.3. Activity measurements

The catalytic combustion of vinyl chloride (VC) was evaluated in a fixed-bed quartz reactor at atmospheric pressure. 0.24 g of the catalyst was used in each experiment. All catalysts were sieved to 40–60 mesh before experiments. The reaction feed gas was composed of dry air (114 mL/min) and 2 vol % vinyl chloride (6 mL/min). The WHSV of the catalytic tests was kept in 30,000 mL g^{-1} h^{-1}. The reaction temperature was increased from 100 °C to 400 °C with a step size of 20 °C, and at each typical temperature point, the reaction conditions were stabilised for 40 min. The composition of effluent gas was analysed online continuously every 4 min by a Ruimin 2060 gas chromatograph. The vinyl chloride (VC) conversion was determined by the following equation:

$$X_{VC}(\%) = \frac{[VC]_{in} - [VC]_{out}}{[VC]_{in}} \times 100$$

where $[VC]_{in}$ and $[VC]_{out}$ denote the concentration of vinyl chloride in the inlet and off-gas, respectively. The selectivity of polychlorinated byproducts (S_{PB}) over the samples was determined by the equation:

$$S_{PB} = \frac{([CH_2Cl_2] + [C_2H_2Cl_2] + [C_2H_4Cl_2]) \times 2 + [C_2H_3Cl_3] \times 3 + [CCl_4] \times 4}{[VC]_{in} \times R_T}$$

where S_{PB} denotes the selectivity of the total chlorine byproducts; $[CH_2Cl_2]$, $[C_2H_2Cl_2]$, $[C_2H_4Cl_2]$, $[C_2H_3Cl_3]$ and $[CCl_4]$ denote the concentrations of CH_2Cl_2, $C_2H_2Cl_2$, $C_2H_4Cl_2$, $C_2H_3Cl_3$ and CCl_4 in the outlet gas, respectively; $[VC]_{in}$ denotes the concentration of vinyl chloride in the inlet gas; and R_T denotes the conversion of vinyl chloride at a specific temperature.

The reaction rates of VC oxidation over the SrCo catalysts were calculated using the following equation:

$$\text{Rate} = \frac{(V_{VC} \div 22.4) \times X_T}{m}$$

where V_{VC} denotes the volume of VC in the inlet gas; X_T denotes the

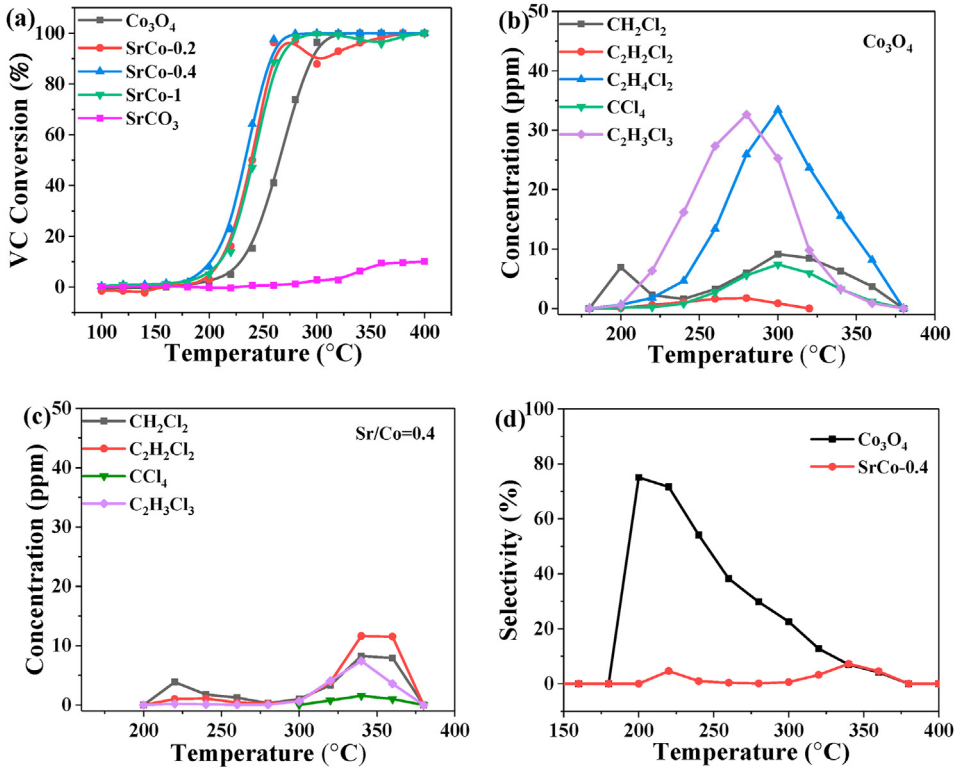

Fig. 1. (a) VC conversion curves over the $SrCO_3$–Co_3O_4 composite catalysts with different molar ratios of Sr/Co. (b) Concentrations of chlorinated byproducts as a function of temperature over the (b) Co_3O_4 and (c) SrCo-0.4 catalysts.(d)The selectivity to polychlorinated byproducts as a function of temperature over the Co_3O_4 and SrCo-0.4 catalysts. The feed gas consisted of 1000 ppm VC and air balance, and the WHSV was 30,000 mL g^{-1} h^{-1}.

Table 1
Comparison of catalytic activity of the SrCo-0.4 catalyst with those in the references for VC oxidation.

Catalysts	VC concentration (ppm)	WHSV ($mL \cdot g^{-1} \cdot h^{-1}$)	Conversion temperature (°C)	References
Co_3O_4-TP	1000	30,000	240 (T_{50}) 267 (T_{90})	[22]
Co(0.7) CeO_x	1000	12,000	249 (T_{50}) 281 (T_{90})	[24]
Co_3O_4-cubic	1000	48,000	308 (T_{50}) 340 (T_{90})	[25]
Co_3O_4-AP	1000	15,000	251 (T_{50}) 275 (T_{90})	[26]
$RuCoO_x$/Al_2O_3-hms	1000	30,000	310 (T_{50}) 345 (T_{90})	[27]
SrCo-0.4	1000	30,000	232 (T_{50}) 256 (T_{90})	This work

conversion of VC at a specific temperature, and *m* denotes the mass of catalyst. For the calculation of the apparent activation energy, the conversion rate was controlled below 15% to ensure no mass/energy transfer limitation.

3. Results

3.1. Activity and stability

Fig. 1a shows the catalytic activity of the $SrCO_3$–Co_3O_4 composite catalysts for the catalytic oxidation of vinyl chloride. The $SrCO_3$ oxide was inactive for VC oxidation. In contrast, the Co_3O_4 oxide exhibited high catalytic activity for VC oxidation, over which the T_{50} (the temperature needed for 50% conversion) was 264 °C. After strontium carbonate was introduced into the Co_3O_4 catalyst, the catalytic performance of the $SrCO_3$–Co_3O_4 composite catalysts was greatly improved. Specifically, according to the T_{50}, their catalytic performance decreased in the following order: SrCo-0.4 > SrCo-0.2 > SrCo-1. Nearly 100% VC conversion was obtained at 280 °C, and 50% VC conversion was obtained at 232 °C over the SrCo-0.4 catalyst. As shown in Fig. S1, only CO_2 product was detected over the SrCo-0.4 catalyst during VC oxidation reaction. Furthermore, as shown in Table 1, it is noted that compared with other transition metal catalysts in previous literature, the $SrCO_3$–Co_3O_4 composite catalysts had a higher catalytic activity for VC [22,24–27], which was comparable to that of costly precious metal catalysts (Table 1).

On the other hand, for the SrCo-0.2 and SrCo-1 catalysts, a slight decrease in VC activity appeared in the temperature ranges of 300–360 and 320–380 °C, respectively (Fig. 1a). This abnormal degradation of VC conversion can be attributed to the accumulation of hydrochloric acid on the catalyst surface and the subsequent destruction of active surface sites [28]. In contrast, no deactivation occurred during the reaction process over the SrCo-0.4 catalyst. However, as shown in Fig. S2a, a slight deactivation was observed on the SrCo-0.4 catalyst during the two cycle tests for VC oxidation. XRD results (Fig. S2b) showed that the structure of $SrCO_3$ in the SrCo-0.4 catalyst was destroyed after two cycle tests. The phase of $SrCO_3$ disappeared and the phase of $SrCl_2$ appeared, indicating that $SrCO_3$ reacted with HCl to produce $SrCl_2$.

The production of polychlorinated byproducts in the process of CVOCs oxidation was inevitable [29–32]. Thus, the distribution of polychlorinated byproducts generated over the Co_3O_4 and SrCo-0.4 catalysts in the reaction process was investigated (Fig. 1b–d). For the Co_3O_4 catalyst, five byproducts were detected, namely, CH_2Cl_2, $C_2H_2Cl_2$, $C_2H_4Cl_2$, CCl_4 and CH_3Cl_3, and $C_2H_4Cl_2$ and $C_2H_3Cl_3$ were dominant. As proposed in previous works, the production of polychlorinated byproducts over the Co_3O_4 catalyst generally followed the ionic chlorination pathway during the VC oxidation process. Electrophilic reactions easily occur on Co-based catalysts (or other transition metal catalysts) due to

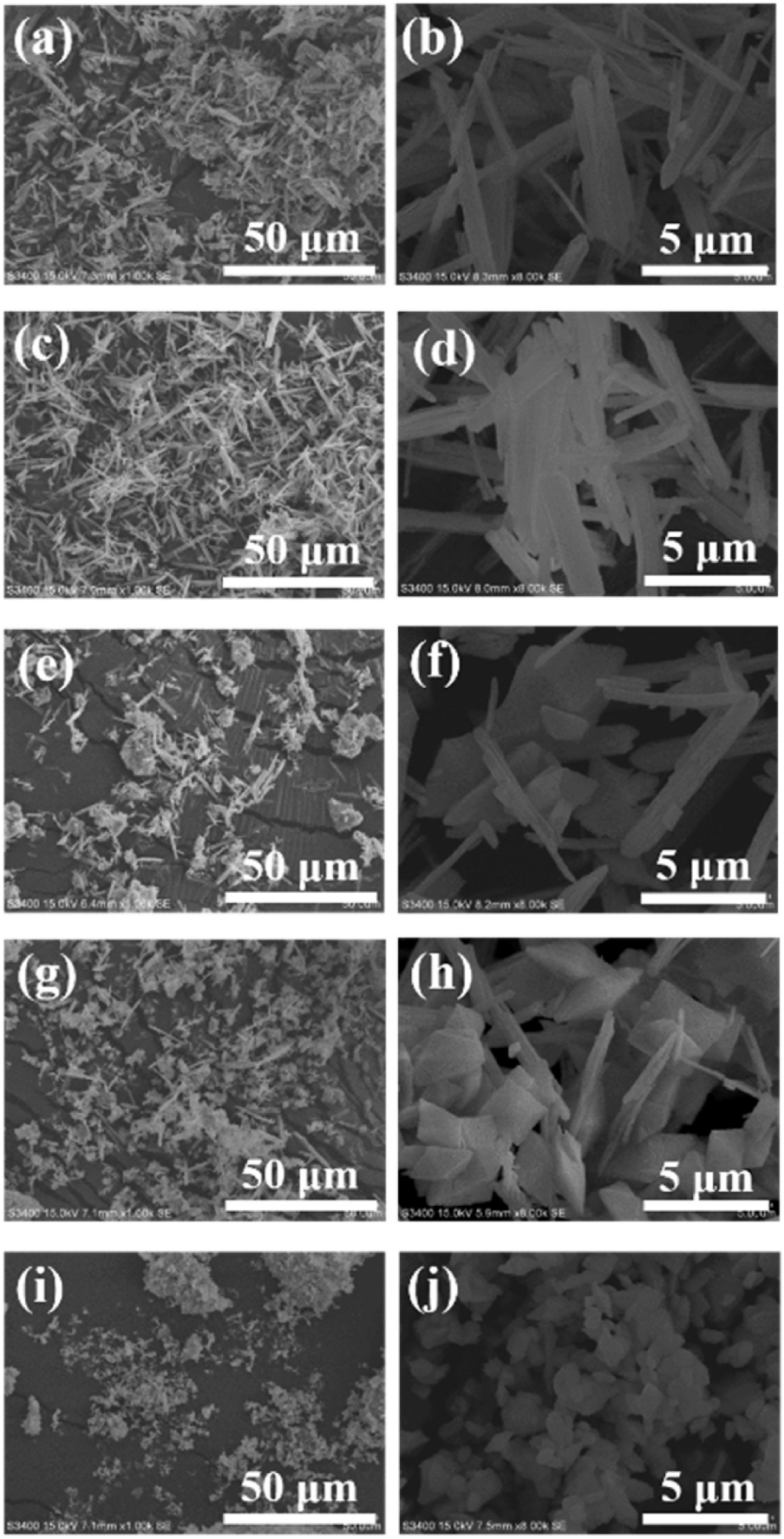

Fig. 2. SEM images of the (a–b) Co_3O_4, (c–d) SrCo-0.2, (e–f) SrCo-0.4, (g–h) SrCo-1 and (i–j) $SrCO_3$ catalysts.

Table 2
Physicochemical properties and redox ability of the $SrCO_3$–Co_3O_4 composite catalysts.

Catalysts	S_{BET} ($m^2 \cdot g^{-1}$)[a]	XPS data			H_2 consumption (mmol/g)[b]		
		BE of Co^{2+} (eV)	BE of Co^{3+} (eV)	Co^{2+}/Co^{3+}	$Co^{3+} \rightarrow Co^{2+}$	$Co^{2+} \rightarrow Co^0$	Co^{2+}/Co^{3+}
$SrCO_3$	8.0	–	–	–	–	–	–
SrCo-1	25.1	781.3	779.7	0.62	3.94	12.52	0.59
SrCo-0.4	40.8	781.4	779.8	0.90	3.58	12.93	0.81
SrCo-0.2	53.4	781.3	779.7	0.68	3.81	12.75	0.67
Co_3O_4	63.5	781.2	779.6	0.55	4.22	12.35	0.46

[a] Measured by the BET method.
[b] Calculated from H_2-TPR profiles after deconvolution and normalization using Co content.

the chlorination of metal atoms into metal chlorides (such as Co-Cl) [33,34]. In other words, the formation of a large number of polychlorinated alkane byproducts was attributed to the chlorination of partial active sites on the Co_3O_4 surface. However, only four byproducts were detected over the SrCo-0.4 catalyst, and their amounts dramatically decreased compared with those over the Co_3O_4 catalyst (Fig. 1c). As shown in Fig. 1d, the selectivity of the SrCo-0.4 catalyst towards the polychlorinated byproducts was much lower than that of the cobalt oxide catalyst, indicating that the introduction of strontium carbonate could restrain the formation of chlorinated byproducts. To reveal the detailed mechanism of their different VC oxidation behaviour, the structural and physicochemical characteristics of the $SrCO_3$–Co_3O_4 composite samples were examined by various characterization methods.

3.2. Catalyst characterization

3.2.1. Structural and compositional analysis

The morphology of the $SrCO_3$–Co_3O_4 composite samples was determined by scanning electron microscopy (SEM). The Co_3O_4 catalyst showed slender rod-shaped particles of approximately 5 μm, as shown in Fig. 2a and b. When $SrCO_3$ was introduced (Fig. 2c and d), slender sticklike particles mainly existed for the SrCo-0.2 catalyst. With increasing $SrCO_3$ content, new small octahedral particles assigned to the $SrCO_3$ phase appeared (Fig. 2e–h). Moreover, the number of slender sticklike particles assigned to Co_3O_4 decreased. As shown in Fig. 2i and j, small particles with various diameters between 1–3 μm were mainly observed for pure $SrCO_3$. Therefore, it was concluded that the morphology of the $SrCO_3$–Co_3O_4 catalysts was dependent on their composition. The specific surface area of all catalysts was detected and is shown in Table 2. Pure Co_3O_4 had a high specific surface area of 63.5 m^2 g^{-1}, while the $SrCO_3$ catalyst had a low specific surface area of 8 m^2 g^{-1}. The specific surface area of the $SrCO_3$–Co_3O_4 catalysts gradually decreased from 63.5 m^2 g^{-1} to 25.1 m^2 g^{-1} as the $SrCO_3$ content increased after the introduction of $SrCO_3$.

Fig. 3a shows the XRD patterns of the $SrCO_3$–Co_3O_4 composite catalysts with various ratios of Sr/Co. For the Co_3O_4 catalyst, there were six diffraction peaks at 19.0°, 31.3°, 36.9°, 44.9°, 59.3° and 65.4°, assigned to a typical spinel structure (JCPDS no. 74–1656) [35]. For the $SrCO_3$ catalyst, the diffraction peaks completely matched the standard card of $SrCO_3$ (JCPDS no. 05–0418), indicating that $SrCO_3$ was successfully synthesized [36]. For the SrCo-0.2, SrCo-0.4 and SrCo-1 composite catalysts, compared with the Co_3O_4 catalyst, the intensity of the characterized diffraction peak at 36.9° gradually decreased, and several peaks at approximately 25.3° appeared and were enhanced with increasing $SrCO_3$ content. In conclusion, the Co_3O_4 and $SrCO_3$ phases existed in the SrCo composite catalysts, and the crystallinity of each oxide decreased by mixing with them. In other words, the introduction of $SrCO_3$ could restrain the crystallization of Co_3O_4, and vice versa.

To further determine the structure of the $SrCO_3$–Co_3O_4 catalysts, the FTIR spectra of all the catalysts were recorded at 400–3000 cm^{-1} and are shown in Fig. 3b. For the Co_3O_4 catalyst, two typical adsorption peaks appeared at 660 and 559 cm^{-1}, assigned to the vibrations of Co^{2+}-O (octahedral site) and Co^{3+}-O (tetrahedral site) [37]. For the $SrCO_3$ catalyst, there was one strong adsorption peak at 1457 and another weak adsorption peak at 859 cm^{-1}, assigned to the bending vibration of CO_3^{2-} in $SrCO_3$ [38]. For the SrCo-0.2, SrCo-0.4 and SrCo-1 catalysts, the adsorption peaks of both the Co_3O_4 and $SrCO_3$ phases appeared at 1457, 859, 660 and 559 cm^{-1}. Furthermore, the intensity of peaks corresponding to Co_3O_4 decreased with increasing $SrCO_3$ content, while that corresponding to the CO_3^{2-} bending vibration increased at the same time. These FTIR results confirmed that the crystallinity of both Co_3O_4 and $SrCO_3$ in the $SrCO_3$–Co_3O_4 catalysts was lower than that in pure Co_3O_4 and $SrCO_3$ according to the XRD results. To further verify the structure of the $SrCO_3$–Co_3O_4 catalysts, the distribution of elements and composition of the $SrCO_3$–Co_3O_4 catalysts were also analysed by EDS mapping. The results shown in Fig. 4 confirmed that Co_3O_4 and $SrCO_3$ phases were present for the $SrCO_3$–Co_3O_4 catalysts. In conclusion, the $SrCO_3$–Co_3O_4 catalysts contained both Co_3O_4 and $SrCO_3$ phases, while their crystallinity decreased due to variable interactions.

3.2.2. XPS

The electronic states of catalyst surface atoms usually have a crucial effect on their catalytic performance [21,39,40]. XPS technology was conducted to detect the change in the valence states of Sr and Co on the catalyst surface. Fig. 5a shows Co 2p3/2 XPS spectra for the $SrCO_3$–Co_3O_4 catalysts with different molar ratios of Sr/Co. The spectra were deconvoluted and fitted to six peaks, representing Co^{3+}, Co^{2+}, and two satellite peaks as marked. Additionally, the binding energy of Co^{3+} gradually shifted from 779.6 eV (Co_3O_4) to 779.8 eV (SrCo-0.4), and the binding energy of Co^{2+} gradually shifted from 781.2 eV (Co_3O_4) to 781.4 eV (SrCo-0.4), indicating that the electron density of Co slightly increased following the introduction of Sr [41]. The binding energy of Co

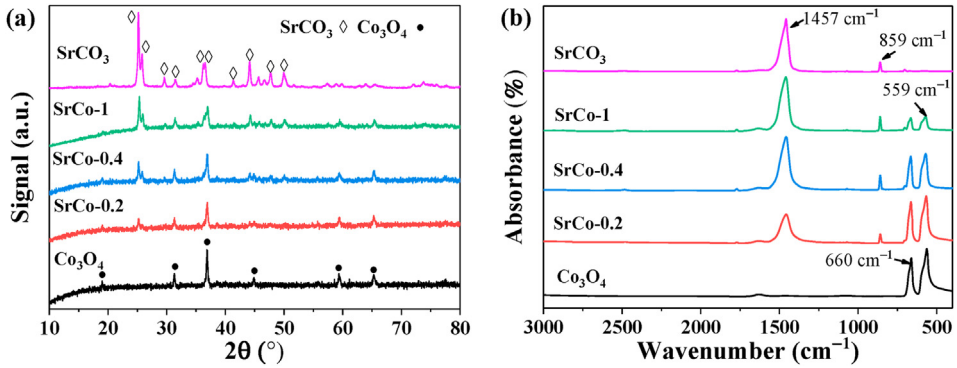

Fig. 3. (a) XRD patterns and (b) FTIR spectra of the $SrCO_3$–Co_3O_4 composite catalysts with different molar ratios of Sr/Co.

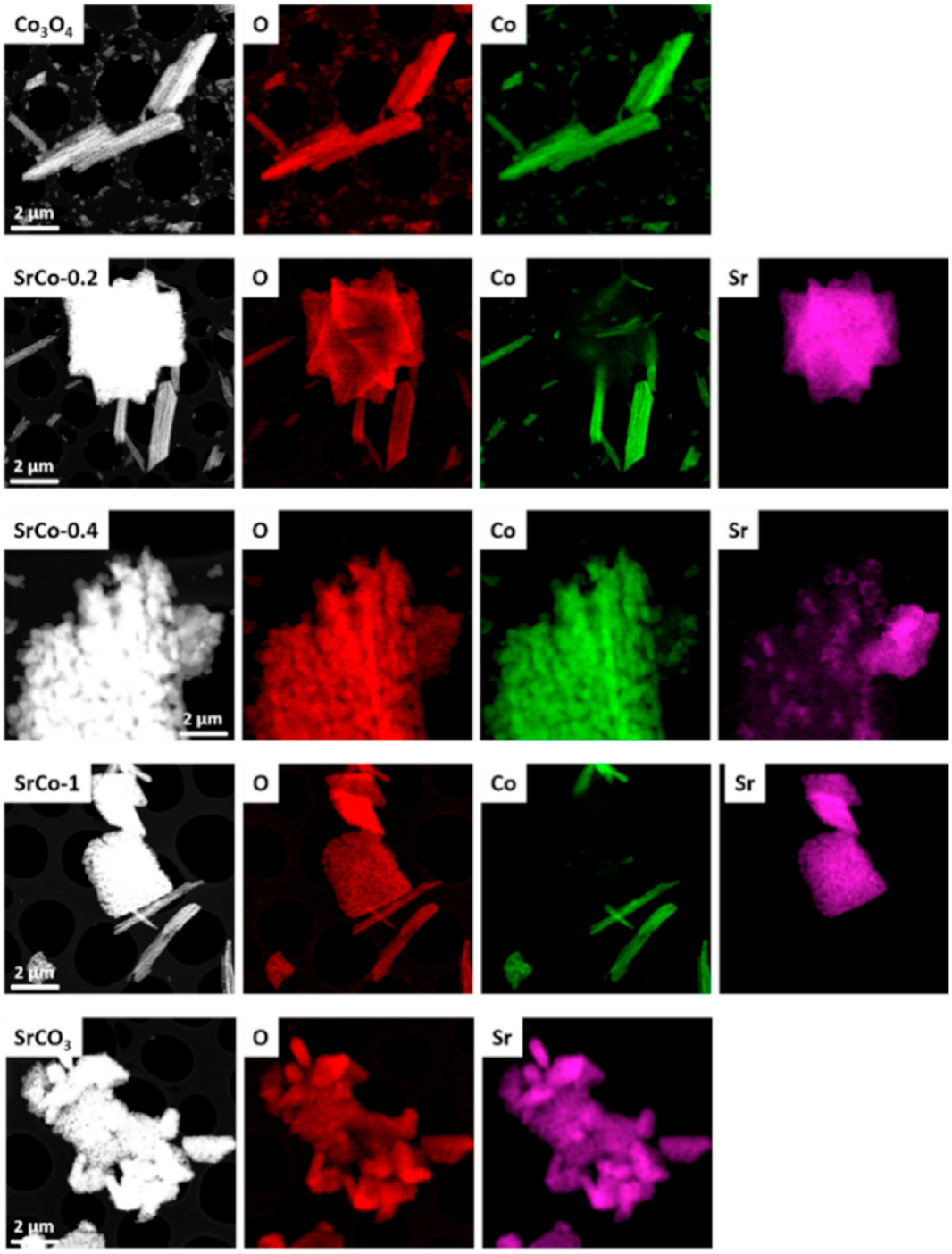

Fig. 4. EDS mapping images of the $SrCO_3$–Co_3O_4 composite catalysts with different molar ratios of Sr/Co.

for the SrCo-1 catalyst was lower than that of the SrCo-0.4 catalyst, which might be explained by reducing the interaction between them based on the excessive proportion of Sr/Co. As a result, the ratio of Co^{2+}/Co^{3+} on the SrCo-x catalyst surface increased after the introduction of $SrCO_3$ and reached the maximum value for the SrCo-0.4 catalyst due to its strongest interaction between Sr and Co-based on the optimized composition. On the other hand, the signal strength of Sr 3d for the SrCo-x catalysts decreased with increasing Co content (Fig. 5b). Moreover, the binding energy of Sr $3d_{5/2}$ shifted from 133.4 eV ($SrCO_3$) to 133.6 eV (SrCo-0.2) [42,43]. In conclusion, the strong interaction between $SrCO_3$ and Co_3O_4 with electron transfer from Sr to Co was proved, which was beneficial to producing a lower valence state of Co, such as more Co^{2+} or $Co^{3-\delta}$ [44].

3.2.3. H_2-TPR and VC-TPD

To reveal the redox properties of the $SrCO_3$–Co_3O_4 catalysts, H_2-TPR technologies were operated in the temperature range of 100–500 °C. As shown in Fig. 6a, no reduction peaks appeared over the pure $SrCO_3$ catalyst, while the pure Co_3O_4 catalyst showed two overlapping reduction peaks at 298 °C and 369 °C, which were ascribed to the reduction of Co^{3+} to Co^{2+} and Co^{2+} to Co^0, respectively [25]. After $SrCO_3$ was added, the two reduction peaks shifted towards lower temperatures of 279 °C and 352 °C for the SrCo-0.2 catalyst. For the SrCo-0.4 catalyst, two reduction peaks further moved towards low temperatures of 260 °C and 330 °C. However, for the SrCo-1 catalyst, two reduction peaks moved to high temperatures of 289 °C and 350 °C. On the other hand, the area of

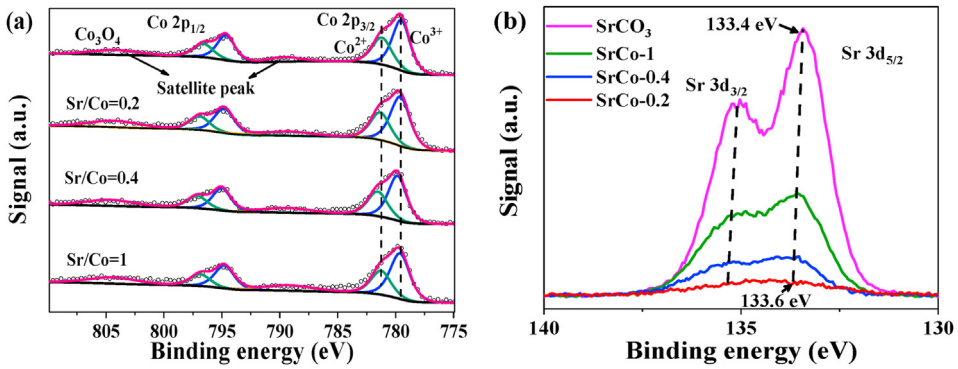

Fig. 5. XPS spectra of (a) Co 2p and (b) Sr 3d for the $SrCO_3$–Co_3O_4 composite catalysts with different molar ratios of Sr/Co.

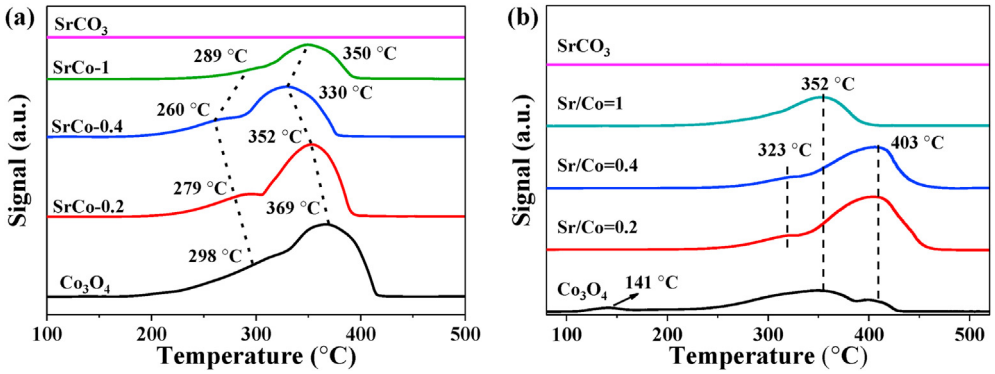

Fig. 6. (a) H_2-TPR and (b) VC-TPD profiles of the $SrCO_3$–Co_3O_4 composite catalysts with different molar ratios of Sr/Co.

reduction peaks decreased with increasing $SrCO_3$ content (Table 2), which was ascribed to the decrease in Co content. It was noted that, compared with the area of reduction peaks, the reduction temperature was the decisive factor affecting the reducibility of catalysts [8,18,22]. Therefore, the reducibility of the $SrCO_3$–Co_3O_4 catalysts declined in the following order: SrCo-0.4 > SrCo-0.2 > SrCo-1 > Co_3O_4. Interestingly, $SrCO_3$ could enhance the reducibility of the Co_3O_4 catalyst, even if it had no redox property. The highest reducibility of the SrCo-0.4 catalyst might be ascribed to a strong interaction between $SrCO_3$ and Co_3O_4 based on the optimized composition, as shown in the XPS results. Furthermore, the actual H_2 consumption of the $SrCO_3$–Co_3O_4 catalysts was carefully calculated after deconvolution and normalization using Co content. In conclusion, the Co^{2+}/Co^{3+} ratio decreased in the following order: SrCo-0.4 (0.81) > SrCo-0.2 (0.67) > SrCo-1 (0.59) > Co_3O_4 (0.46), in according with the XPS results.

In addition to redox properties, the adsorption capacity of the catalyst for vinyl chloride (VC) also plays a critical role in VC oxidation. Hence, a VC-TPD experiment was implemented to determine the VC adsorption capacity of the $SrCO_3$–Co_3O_4 samples. Three overlapping peaks appeared at 141, 352 and 403 °C for the Co_3O_4 catalyst (Fig. 6b). After the addition of $SrCO_3$, the VC desorption peak at 141 °C disappeared for the SrCo-0.2 catalyst, and the area of the peak at 403 °C significantly increased. For the SrCo-0.4 catalyst, the desorption curve was similar to that for the SrCo-0.2 catalyst, except for the larger peak area at 403 °C. However, as the $SrCO_3$ content further increased, only one peak at 352 °C appeared for the SrCo-1 sample, and the desorption peak at 403 °C disappeared. The total peak area decreased in the following order: SrCo-0.4 (2.41) > SrCo-0.2 (1.76) > Co_3O_4 (1.32) > SrCo-1 (0.97). The low amount of VC desorption for the SrCo-1 catalyst was ascribed to the lower Co content of the catalyst. Therefore, the VC adsorption ability of the $SrCO_3$–Co_3O_4 samples decreased in the following order: SrCo-0.4 > SrCo-0.2 > Co_3O_4 > SrCo-1 > $SrCO_3$. Although the $SrCO_3$ catalyst was unable to adsorb vinyl chloride, it could enhance the VC adsorption capacity of the $SrCO_3$–Co_3O_4 catalysts by tuning the crystallinity and electronic state of Co on the surface of the catalyst.

4. Discussion

The VC adsorption capacity and redox ability play decisive roles in VC oxidation [21]. VC adsorption was the first step of the oxidation reaction, facilitating the subsequent dechlorination reaction. The redox ability was responsible for the oxidation of the intermediate species generated after dechlorination. Therefore, enhancing the capability for VC adsorption and the reducibility for Co_3O_4 is a key issue to improve its catalytic performance for VC oxidation.

$SrCO_3$–Co_3O_4 composite catalysts with different ratios of Sr/Co were synthesized by the coprecipitation method. XRD, FTIR and SEM results revealed that the $SrCO_3$–Co_3O_4 catalysts were composed of $SrCO_3$ and Co_3O_4 phases, and the presence of $SrCO_3$ could restrain the crystallization of Co_3O_4, possibly due to intimate contact between the two components. Furthermore, XPS results showed that electron transfer from Sr to Co was present on the $SrCO_3$–Co_3O_4 catalysts, generating electron-rich Co (Co^{2+} and $Co^{3-\delta}$) on the Co_3O_4 surface. To further explore the impact of adding $SrCO_3$ on the chemical properties of the $SrCO_3$–Co_3O_4 composite samples, H_2-TPR and VC-TPD technologies were used to determine the redox properties and VC adsorption capacity of the samples, respectively. H_2-TPR results indicated that $SrCO_3$ could promote the reducibility of the Co_3O_4 catalyst, and the SrCo-0.4 catalyst showed the strongest reducibility among the SrCo catalysts. Moreover, the introduction of $SrCO_3$ could enhance the VC adsorption ability of the SrCo-0.2 and SrCo-0.4 catalysts.

In summary, for the SrCo-0.2 and SrCo-0.4 catalysts, the incorporation of $SrCO_3$ promoted the reducibility and VC adsorption capacity of the catalysts by reducing the crystallinity and tuning the state of Co on the surface of the catalyst, resulting in significant promotion of the catalytic activity for vinyl chloride oxidation. The E_a for VC oxidation

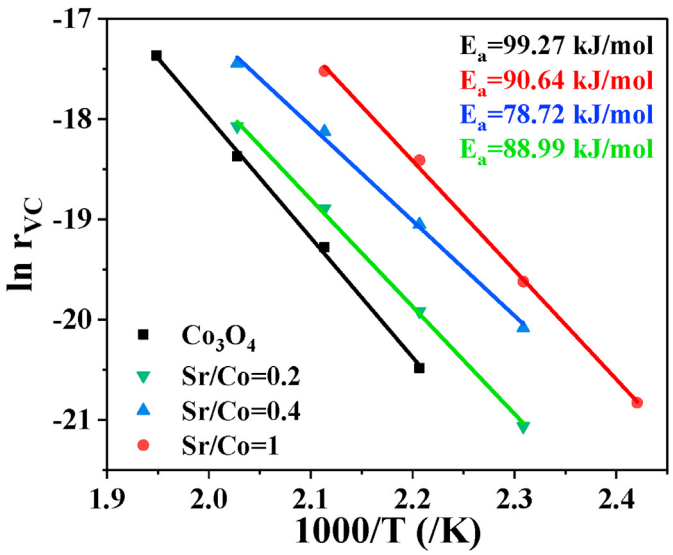

Fig. 7. Arrhenius plots for VC oxidation over the $SrCO_3$–Co_3O_4 composite catalysts with different molar ratios of Sr/Co.

Table 3
Catalytic activity data of the $SrCO_3$–Co_3O_4 catalysts in VC oxidation.

Catalysts	Ea (kJ/mol)[a]	$r_{VC} \times 10^8$ (mol g^{-1} s^{-1})[b]	$r_{VC} \times 10^9$ (s^{-1})[c]	TOF $\times 10^9$ (mol m^{-2} s^{-1})[d]
SrCo-1	90.64	0.97	10.7	0.18
SrCo-0.4	78.72	1.34	18.6	0.33
SrCo-0.2	88.99	0.62	14.1	0.25
Co_3O_4	99.27	0.42	3.36	0.07

[a] VC conversion was kept below 15%.
[b] VC conversion was below 10% at 200 °C.
[c] VC conversion lower than 10% at 200 °C per mole of Co.
[d] VC conversion lower than 10% at 200 °C per unit of surface area.

increased in the following order: SrCo-0.4 (78.72 kJ/mol) < SrCo-0.2 (88.99 kJ/mol) < SrCo-1 (90.64 kJ/mol) < Co_3O_4 (99.27 kJ/mol) (Fig. 7 and Table 3). Moreover, the SrCo catalysts exhibited a higher reaction rate and TOF than the Co_3O_4 catalyst, confirming the high efficiency of the SrCo catalysts. It was noted that the catalytic activity of the SrCo-1 catalyst was slightly lower than that of the SrCo-0.4 and SrCo-0.2 catalysts, which may be ascribed to the weak interaction between $SrCO_3$ and Co_3O_4 phases based on the ultrahigh Sr/Co ratio. Consequently, the reducibility and VC adsorption ability of the SrCo-1 catalyst were weakened, leading to a higher E_a than that of the SrCo-0.4 and SrCo-0.2 catalysts.

5. Conclusions

$SrCO_3$–Co_3O_4 composite catalysts with different ratios of Sr/Co were prepared by the coprecipitation method. The introduction of $SrCO_3$ could restrain the crystallization of Co_3O_4 and increase the electron density of Co on the catalyst surface due to the interaction between $SrCO_3$ and Co_3O_4. Moreover, this interaction could enhance the reducibility and VC adsorption ability of the $SrCO_3$–Co_3O_4 catalysts compared with the Co_3O_4 catalyst. Furthermore, among the $SrCO_3$–Co_3O_4 catalysts, the SrCo-0.4 catalyst had the highest reducibility and adsorption ability, resulting in its highest catalytic activity presented with the highest reaction rate and lowest apparent activation energy. This work offered a new strategy for designing highly efficient Co_3O_4-based catalysts for eliminating chlorinated volatile organic compounds.

Declaration of competing interest

The authors declare that they have no known competing financial interests or personal relationships that could have appeared to influence the work reported in this paper.

Acknowledgments

This study was financially supported by the National Key Research and Development Program of China (2016YFC0204300), the National Natural Science Foundation of China (21922602, 22076047, 21976057), the Shanghai Science and Technology Innovation Action Plan (20dz1204200) and Fundamental Research Funds for the Central Universities.

Appendix A. Supplementary data

Supplementary data to this article can be found online at https://doi.org/10.1016/j.jics.2021.100116.

References

[1] Ma X, Zhao M, Pang Q, Zheng M, Sun H, Crittenden J, Zhu Y, Chen Y. Development of novel $CaCO_3/Fe_2O_3$ nanorods for low temperature 1,2-dichlorobenzene oxidation. Appl. Catal. Gen. 2016;522:70–9. https://doi.org/10.1016/j.apcata.2016.04.025.
[2] Cheng Z, Li J, Yang P, Zuo S. Preparation of MnCo/MCM-41 catalysts with high performance for chlorobenzene combustion. Chin. J. Catal. 2018;39:849–56. https://doi.org/10.1016/S1872-2067(17)62950-4.
[3] Wang L, Xie H, Wang X, Zhang G, Guo Y, Guo Y, Lu G. Preparation of $LaMnO_3$ for catalytic combustion of vinyl chloride. Chin. J. Catal. 2017;38:1406–12. https://doi.org/10.1016/S1872-2067(17)62863-8.
[4] Dai Q, Zhang Z, Yan J, Wu J, Johnson G, Sun W, Wang X, Zhang S, Zhan W. Phosphate-functionalized CeO_2 nanosheets for efficient catalytic oxidation of dichloromethane. Environ. Sci. Technol. 2018;52:13430–7. https://doi.org/10.1021/acs.est.8b05002.
[5] Dai Q, Wu J, Deng W, Hu J, Wu Q, Guo L, Sun W, Zhan W, Wang X. Comparative studies of P/CeO_2 and Ru/CeO_2 catalysts for catalytic combustion of dichloromethane: from effects of H_2O to distribution of chlorinated by-products. Appl. Catal., B 2019;249:9–18. https://doi.org/10.1016/j.apcatb.2019.02.065.
[6] Dai Q, Shen K, Deng W, Cai Y, Yan J, Wu J, Guo L, Liu R, Wang X, Zhan W. HCl-Tolerant H_xPO_4/RuO_x–CeO_2 catalysts for extremely efficient catalytic elimination of chlorinated VOCs. Environ. Sci. Technol. 2021;55:4007–16. https://doi.org/10.1021/acs.est.0c08256.
[7] Yang P, Yang S, Shi Z, Meng Z, Zhou R. Deep oxidation of chlorinated VOCs over CeO_2-based transition metal mixed oxide catalysts. Appl. Catal., B 2015;162:227–35. https://doi.org/10.1016/j.apcatb.2014.06.048.
[8] Hua W, Zhang C, Guo Y, Chai G, Wang C, Guo Y, Wang L, Wang Y, Zhan W. An efficient $Sn_yMn_{1-y}O_x$ composite oxide catalyst for catalytic combustion of vinyl chloride emissions. Appl. Catal., B 2019;255:117748.
[9] Yang P, Zuo S, Shi Z, Tao F, Zhou R. Elimination of 1,2-dichloroethane over $(Ce,Cr)_xO_2/MO_y$ catalysts (M = Ti, V, Nb, Mo, W and La). Appl. Catal., B 2016;191:53–61. https://doi.org/10.1016/j.apcatb.2016.03.017.
[10] Zhang C, Wang C, Zhan W, Guo Y, Guo Y, Lu G, Baylet A, Giroir-Fendler A. Catalytic oxidation of vinyl chloride emission over $LaMnO_3$ and $LaB_{0.2}Mn_{0.8}O_3$(B = Co, Ni, Fe) catalysts. Appl. Catal., B 2013;129:509–16. https://doi.org/10.1016/j.apcatb.2012.09.056.
[11] Lu Y, Dai Q, Wang X. Catalytic combustion of chlorobenzene on modified $LaMnO_3$ catalysts. Catal. Commun. 2014;54:114–7. https://doi.org/10.1016/j.catcom.2014.05.018.
[12] Zhang X, Liu Y, Deng J, Yu X, Han Z, Zhang K, Dai H. Alloying of gold with palladium: an effective strategy to improve catalytic stability and chlorine-tolerance of the 3DOM CeO_2-supported catalysts in trichloroethylene combustion. Appl. Catal., B 2019;257:117879. https://doi.org/10.1016/j.apcatb.2019.117879.
[13] Aranzabal A, Pereda-Ayo B, González-Marcos MP, González-Marcos JA, López-Fonseca R, González-Velasco JR. State of the art in catalytic oxidation of chlorinated volatile organic compounds. Chem. Pap. 2014;68:1169–86. https://doi.org/10.2478/s11696-013-0505-7.
[14] He C, Cheng J, Zhang X, Douthwaite M, Pattisson S, Hao Z. Recent advances in the catalytic oxidation of volatile organic compounds: a review based on pollutant sorts and sources. Chem. Rev. 2019;119:4471–568. https://doi.org/10.1021/acs.chemrev.8b00408.
[15] Zhan W, Guo Y, Gong X, Guo Y, Wang Y, Lu G. Current status and perspectives of rare earth catalytic materials and catalysis. Chin. J. Catal. 2014;35:1238–50. https://doi.org/10.1016/S1872-2067(14)60189-3.
[16] Zhang C, Wang C, Hua W, Guo Y, Lu G, Gil S, Giroir-Fendler A. Relationship between catalytic deactivation and physicochemical properties of $LaMnO_3$ perovskite catalyst during catalytic oxidation of vinyl chloride. Appl. Catal., B 2016;186:173–83. https://doi.org/10.1016/j.apcatb.2015.12.052.

[17] He C, Pan K, Chang M. Catalytic oxidation of trichloroethylene from gas streams by perovskite-type catalysts. Environ. Sci. Pollut. Res. 2018;25:11584–94. https://doi.org/10.1007/s11356-018-1440-5.
[18] Huang H, Gu Y, Zhao J, Wang X. Catalytic combustion of chlorobenzene over VO_x/CeO_2 catalysts. J. Catal. 2015;326:54–68. https://doi.org/10.1016/j.jcat.2015.02.016.
[19] Deng W, Dai Q, Lao Y, Shi B, Wang X. Low temperature catalytic combustion of 1,2-dichlorobenzene over CeO_2–TiO_2 mixed oxide catalysts. Appl. Catal., B 2016;181:848–61. https://doi.org/10.1016/j.apcatb.2015.07.053.
[20] Cai T, Huang H, Deng W, Dai Q, Liu W, Wang X. Catalytic combustion of 1,2-dichlorobenzene at low temperature over Mn-modified Co_3O_4 catalysts. Appl. Catal., B 2015;166–167:393–405. https://doi.org/10.1016/j.apcatb.2014.10.047.
[21] Liu H, Li X, Dai Q, Zhao H, Chai G, Guo Y, Guo Y, Wang L, Zhan W. Catalytic oxidation of chlorinated volatile organic compounds over Mn-Ti composite oxides catalysts: elucidating the influence of surface acidity. Appl. Catal., B 2021;282:119577. https://doi.org/10.1016/j.apcatb.2020.119577.
[22] Yuan C, Liu S, Wang Z, Wang G. Catalytic oxidation of low concentrations of vinyl chloride over spinel-type Co_3O_4 catalysts. React. Kinet. Mech. Catal. 2018;125:757–71. https://doi.org/10.1007/s11144-018-1449-2.
[23] Wang C, Zhang C, Hua W, Guo Y, Lu G, Gil S, Giroir-Fendler A. Low-temperature catalytic oxidation of vinyl chloride over Ru modified Co_3O_4 catalysts. RSC Adv. 2016;6:99577–85. https://doi.org/10.1039/c6ra18503g.
[24] Wang C, Zhang C, Hua W, Guo Y, Lu G, Gil S, Giroir-Fendler A. Catalytic oxidation of vinyl chloride emissions over Co-Ce composite oxide catalysts. Chem. Eng. J. 2017;315:392–402. https://doi.org/10.1016/j.cej.2017.01.007.
[25] Wang C, Hua W, Chai G, Zhang C, Guo Y. Insights into the morphological effect of Co_3O_4 crystallite on catalytic oxidation of vinyl chloride. Catalysts 2019;9:1–10. https://doi.org/10.3390/catal9050408.
[26] Hua W, Li M, Guo Y, Chai G, Liu H, Guo Y, Wang L, Zhan W. Catalytic combustion of vinyl chloride emissions over Co_3O_4 catalysts with different crystallite sizes. Rare Met. 2020. https://doi.org/10.1007/s12598-020-01512-3.
[27] Wang C, Liu N, Zhang C, Liu X, Li X, Zhao X. Ruthenium/cobalt binary oxides supported on hollow alumina microspheres as highly efficient catalyst for vinyl chloride oxidation. Appl. Surf. Sci. 2019;497:143776. https://doi.org/10.1016/j.apsusc.2019.143776.
[28] Pitkäaho S, Matejova L, Jiratova K, Ojala S, Keiski RL. Oxidation of perchloroethylene—activity and selectivity of Pt, Pd, Rh, and V_2O_5 catalysts supported on Al_2O_3, Al_2O_3–TiO_2 and Al_2O_3–CeO_2. Part 2. Appl. Catal., B 2012;126:215–24. https://doi.org/10.1016/j.apcatb.2012.07.025.
[29] de Rivas B, López-Fonseca R, Gutiérrez-Ortiz MÁ, Gutiérrez-Ortiz JI. Structural characterisation of $Ce_{0.5}Zr_{0.5}O_2$ modified by redox treatments and evaluation for chlorinated VOC oxidation. Appl. Catal., B 2011;101:317–25. https://doi.org/10.1016/j.apcatb.2010.09.034.
[30] Wan Y, Zhang C, Guo Y, Guo Y, Lu G. Catalytic combustion of vinyl chloride emission over CeO_2-MnO_x Catalyst. Chin. J. Catal. 2012;33:557–62. https://doi.org/10.3724/SP.J.1088.2012.11003.
[31] Liu H, Yang J, Jia Y, Wang Z, Jiang M, Shen K, Zhao H, Guo Y, Guo Y, Wang L, Dai S, Zhan W. Significant improvement of catalytic performance for chlorinated volatile organic compound oxidation over RuO_x supported on acid-etched Co_3O_4. Environ. Sci. Technol. 2020. https://doi.org/10.1021/acs.est.1c02970.
[32] Shi Y, Guo X, Shi Z, Zhou R. Transition metal doping effect and high catalytic activity of CeO_2-TiO_2 for chlorinated VOCs degradation. J. Rare Earths 2021. https://doi.org/10.1016/j.jre.2021.02.005.
[33] Doyle MP, Siegfried B, Dellaria JF. Alkyl nitrite-metal halide deamination reactions. 2. substitutive deamination of arylamines by alkyl nitrites and copper(II) halides. A direct and remarkably efficient conversion of arylamines to aryl halides. J. Org. Chem. 1977;42:2426–31. https://doi.org/10.1021/jo00434a017.
[34] Taylor PH, Sidhu SS, Rubey WA, Dellinger B, Wehrmeier A, Lenoir D, Schramm KW. Evidence for a unified pathway of dioxin formation from aliphatic hydrocarbons. Symp. Combust. 1998;27:1769–75. https://doi.org/10.1016/S0082-0784(98)80018-0.
[35] Ren Q, Mo S, Peng R, Feng Z, Zhang M, Chen L, Fu M, Wu J, Ye D. Controllable synthesis of 3D hierarchical Co_3O_4 nanocatalysts with various morphologies for the catalytic oxidation of toluene. J. Mater. Chem. A. 2018;6:498–509. https://doi.org/10.1039/c7ta09149d.
[36] Xu Y, Zhong X, Li Y, Liu J. Morphology-controllable self-assembly of strontium carbonate ($SrCO_3$) crystals under the action of different regulators. J. Mater. Sci. Mater. Electron. 2019;30:21150–9. https://doi.org/10.1007/s10854-019-02487-3.
[37] Ji L, Lin J, Zeng H. Metal-support interactions in Co/Al_2O_3 catalysts: a comparative study on reactivity of support. J. Phys. Chem. B 2000;104:1783–90. https://doi.org/10.1021/jp993400l.
[38] Ghouri ZK, Elsaid K, Al-Meer S, Barakat NAM. Applicable anode based on Co_3O_4–$SrCO_3$ heterostructure nanorods-incorporated cnfs with low-onset potential for dufcs. Appl. Nanosci. 2017;7:625–31. https://doi.org/10.1007/s13204-017-0601-z.
[39] Ding Y, Wu Q, Lin B, Guo Y, Guo Y, Wang Y, Wang L, Zhan W. Superior catalytic activity of a Pd catalyst in methane combustion by fine-tuning the phase of ceria-zirconia support. Appl. Catal., B 2020;266:118631. https://doi.org/10.1016/j.apcatb.2020.118631.
[40] Hu Z, Qiu S, You Y, Guo Y, Guo Y, Wang L, Zhan W, Lu G. Hydrothermal synthesis of $NiCeO_x$ nanosheets and its application to the total oxidation of propane. Appl. Catal., B 2018;225:110–20. https://doi.org/10.1016/j.apcatb.2017.08.068.
[41] Dai L, Lu X, Chu G, He C, Zhan W, Zhou G. Surface tuning of $LaCoO_3$ perovskite by acid etching to enhance its catalytic performance. Rare Met. 2020. https://doi.org/10.1007/s12598-019-01360-w.
[42] Li Q, Pan H, Zhu C, Xu P, Zhang X. Substitution effect of Sn for Cu in the $Bi_2Sr_2CaCu_{2-x}Sn_xO_{8+\delta}$ system. J. Supercond. Nov. Magnetism 2000;13:137–9. https://doi.org/10.1023/A:1007794613891.
[43] Zhang Y, Chen XY, Xie B, Wang Z, Ding M, He Q, Ji H, Mo TL, Yu P. Leakage current characteristics of $SrTiO_3$/$LaNiO_3$/$Ba_{0.67}Sr_{0.33}TiO_3$/$SrTiO_3$ heterostructure thin films. Rare Met. 2021;40:961–7. https://doi.org/10.1007/s12598-020-01497-z.
[44] Guo Z, Wang Y, Li M, Wang S, Du F. Vulcanization and acid etching of NiCoFe layered ternary hydroxides for enhancing oxygen evolution reaction. J. Alloys Compd. 2020;832:155012. https://doi.org/10.1016/j.jallcom.2020.155012.